Structures 71 (2025) 108197

Contents lists available at ScienceDirect

Structures

journal homepage: www.elsevier.com/locate/structures

Effectiveness of SRG in shear strengthening of deep and slender concrete beams

Xiangsheng Liu [a,*], Georgia E. Thermou [b]

[a] Centre for Structural Engineering and Informatics, Dept. of Civil Engineering, The University of Nottingham, Nottingham NG7 2RD, UK
[b] Structural Engineering, Dept. of Civil Engineering, The University of Nottingham, Nottingham NG7 2RD, UK

ARTICLE INFO

Keywords:
Beam
Mortar-based Composites
Shear Strengthening
FRCM
SRG
Shear Span-to-Depth Ratio

ABSTRACT

This study investigates Steel-Reinforced Grout (SRG) jackets' efficiency in enhancing the shear strength in Reinforced Concrete (RC) beams with various shear span-to-depth (a/d) ratios, comparing them with Carbon Fabric Reinforced Cementitious Mortars (CFRCM) and Steel Reinforced Polymer (SRP) jackets. Seventeen beams underwent monotonic loading to assess the impact of the textile layer number and jacket configuration for a/d= 2.0 and 3.5. The results demonstrated that SRG, CFRCM, and SRP systems increased the shear strength by up to 124 %, 174 %, and 176 % for deep beams (a/d = 2.0) and 170 %, 215 %, and 221 % for slender beams (a/d = 3.5), respectively. Fully wrapped SRG and SRP systems shifted failure from brittle to ductile. An analytical model is proposed for predicting SRG strengthened beam shear capacity, accounting for the influence of a/d, with a correlation coefficient (R^2) of 95.84 %.

1. Introduction

The performance of existing reinforced concrete (RC) structures can be significantly affected by various factors, including material ageing (e.g., steel corrosion), poor construction quality, and most importantly, inadequate reinforcement detailing, such as widely spaced stirrups [1–3]. The latter significantly influences the provided level of passive confinement, directly impacting the ductility of existing RC columns and beams as well as their shear resistance [4,5]. These inherent deficiencies become particularly pronounced during seismic events, potentially leading to shear failure - a frequent cause of abrupt, catastrophic collapses endangering both lives and structures [2,6].

With advancements in material technology, Fiber Reinforced Polymers (FRP) have been widely utilized in concrete structures as internal reinforcement [7–11]. Moreover, FRPs are also extensively employed as externally bonded reinforcement for flexural and shear strengthening, due to its ease of application, fast implementation, light weight, and non-invasiveness. However, the epoxy resin matrix in FRP systems encounters performance challenges at high temperatures, is costly, cannot be applied to wet surfaces, and lacks compatibility with concrete. To overcome these issues, a new generation of composite materials has emerged, the Fabric Reinforced Cementitious Mortars (FRCMs), where the resin has been substituted by mortar [12,13]. The most popular systems are the Textile Reinforced Mortar (TRM) with continuous carbon, basalt, or glass fibre (B-, C-, GFRCM) [14–26], and the Polipar-afenilen Benzobisoxazole (PBO)-FRCM using PBO net [14–17, 27–30]. The fibres and textiles used in TRM and PBO-FRCM composites are relatively expensive, which has prompted the development of a new, economically efficient composite material, the Steel-Reinforced Grout (SRG) as an alternative [31,32]. In SRG, Ultra-High Tensile Strength Steel (UHTSS) are embedded into the mortar.

Recently, Liu and Thermou [33] conducted a review of the current state of research on shear strengthening of RC beams retrofitted using mortar-based composites. FRCM jacketing has shown the potential to significantly increase shear capacity by up to 196 % compared to control beams. This enhancement comes with various potential failure modes, including FRCM detachment, fibre fracture, and slippage through the mortar interface. The effectiveness of shear strengthening was found to be influenced by several key parameters, such as the strengthening configuration, the ratio of matrix-to-concrete strength, and the stiffness of the fibres used. Furthermore, it was demonstrated that current research focuses mainly on Carbon FRCM (CFRCM). Research investigating the use of SRG jacketing is limited in the existing literature on this subject.

Thermou et al. [12] investigated the impact of various configurations of SRG jacketing (U-shaped, fully wrapped), textile densities (1.57 and

* Corresponding author.
E-mail address: evxxl17@nottingham.ac.uk (X. Liu).

https://doi.org/10.1016/j.istruc.2025.108197
Received 27 July 2024; Received in revised form 10 December 2024; Accepted 4 January 2025
Available online 8 January 2025

4.72 cords/cm), the use or no of mechanical anchorage of the textile, and textile layers (one and two) on rectangular beams with a shear span ratio (a/d) equal to 2. The results showed that SRG jacketing effectively improved the shear capacity (up to 160 %), and for the fully wrapped beams the mode of failure changed from shear to flexural. Wakjira and Ebead [31] conducted experimental studies on 11 RC T-section beams with $a/d = 2.8$, reinforced with 1.57 and 3.14 cords/cm UHTSS density SRG jackets. Their test results confirmed the effectiveness of the SRG system, with strengthened beams exhibiting a maximum capacity increase of up to 71 % compared to control beams. They also developed an analytical model based on Simplified Modified Compression Field Theory (SMCFT) to predict the shear capacity of SRG-strengthened beams. However, research in this area is still in its early stages [34]. Existing studies on shear properties of SRG strengthened beams remain limited, particularly regarding comprehensive comparisons with other strengthening systems such as CFRCM and SRP. Additionally, the impact of SRG on failure mode transitions and energy dissipation has not been extensively investigated, leaving significant gaps in understanding its full potential and limitations.

The influence of shear span-to-depth ratio (a/d) on the shear response of reinforced concrete (RC) beams is well-documented by dictating the dominant shear transfer mechanism [35]. At lower a/d ratios (deep beams), shear forces are primarily resisted through arch action, where compressive struts directly transfer forces to the supports. Conversely, as a/d increases (slender beams), the primary load transfer mechanism transitions to truss-like response involving tensile forces in the stirrups and the concrete's tensile strength. This transition profoundly influences the ductility, failure mode, and ultimate shear capacity of the beam. Research [36–38] has shown that lower a/d ratios generally lead to greater shear capacity due to the predominance of arch action, whereas slender beams with higher a/d ratios tend to exhibit reduced shear resistance and increased vulnerability to shear cracking. Moreover, a/d ratios also affect crack propagation patterns, load distribution, and the effectiveness of internal reinforcement, as emphasized in studies [39,40].

For externally strengthened RC beams, current research has demonstrated the impact of a/d on the shear improvement of FRP retrofitted beams [41,42]. Nevertheless, limited and inconclusive studies regarding the influence of a/d on FRCM jacketed beams exist, with only two studies offering conflicting conclusions [16,27]. Tetta et al. [21] compared the shear enhancement effects of different textile (glass, carbon, basalt) in TRM beams across a/d ratios of 1.6, 2.6, and 3.6. Their findings supported the conclusion that changes in a/d ratio do not influence the shear strength provided by TRM jackets. Wakjira and Ebead [32] studied the shear performance of U-shaped SRG-jacketed beams across different a/d ratios (1.6, 2.1, 2.6, and 3.1). Their three-point bending tests confirmed that a/d significantly enhances the shear strengthening effect of SRG in deep beams ($a/d \leq 2.5$) but deteriorates in slender beams ($a/d > 2.5$). Given the critical role of the a/d ratio in influencing shear transfer mechanisms, failure modes, and retrofitting efficiency, along with the limited and conflicting findings in existing literature, this study aims to address the gap in understanding the interaction between a/d ratios and the performance of SRG jacketing systems.

Therefore, this paper aims to investigate the efficiency of SRG jacketing in enhancing the shear strength of deficient deep ($a/d = 2$) and slender ($a/d = 3.5$) RC beams. Additionally, the performance of Steel-Reinforced Polymer (SRP) and CFRCM jacketing systems is assessed for comparison. The impact of the number of textile layers (1–3 layers) and the jacket configuration (U-shaped, fully wrapped) is experimentally investigated on 17 asymmetrically three-point loaded beams. The effectiveness of SRG jacketing in enhancing the shear strength of deficient RC beams is explored and compared with that of other composite systems. This study seeks to extend the understanding of SRG jacketing beyond its shear capacity enhancement by examining its effects on ductility, energy dissipation, and failure mode transitions. Unlike existing research, this work also provides a comparative analysis of SRG systems against other advanced composites such as CFRCM and SRP, offering a holistic perspective on the efficiency of SRG in diverse configurations and scenarios. By proposing an analytical model tailored to SRG-strengthened beams, this study aims to address the lack of predictive tools specific to SRG systems, particularly under varying a/d ratios.

2. Experimental programme

2.1. Specimen details

The experiments included 17 rectangular RC beams tested under three-point bending monotonic loading using a simply supported configuration. The total length is 1677 mm (660 in.), the effective span is 1100 mm, and the breadth × height is 102 mm × 203 mm (40 in. × 80 in.). Two different shear span ratios (a/d) of 2.0 and 3.5 were investigated (Beam series A and B, respectively). Beams with $a/d \leq 2.5$ fall into the classification of deep beams, whereas those exceeding 2.5 are categorized as slender beams [43–45]. To directly evaluate the effectiveness of the SRG and other jacketing systems (such as SRP and CFRCM) considered in this study, no internal transverse reinforcement was included in the critical span (a=350 mm for Series A and a=620 mm for Series B). The remaining span contained 8 mm diameter stirrups spaced at 140 mm and 40 mm for Series A and Series B beams, respectively (Fig. 1(a)). All beams had tensile and compressive longitudinal reinforcements equal to 2 ∅16 and 2 ∅10, respectively (Fig. 1(b)).

The key parameters of this study include the: (a) shear span-to-depth ratios (2.0 and 3.5), (ii) composite strengthening systems, namely SRG, SRP, CFRCM, (iii) density of ultra-high tensile strength steel (UHTSS) textiles, 1.57 and 3.14 cords/in (low density and high density, respectively), (iv) number of textile layers (1–3 layers), and (v) strengthening configuration (fully wrapped and U-wrapped jackets) (Fig. 1(c)).

The details of the beams tested are shown in Table 1. The code name given to the specimens corresponds to X-YZ-Qi, where "X" is equal to A or B corresponding to the beam with $a/d = 2$ or 3.5, respectively. 'Y' indicates the material used for the beam jacketing with N corresponding to non-strengthening, 'G' to SRG jacketing, 'P' to SRP jacketing, and 'C' to CFRCM jacketing. In case of SRP and SRG jacketing, 'Z' is equal to 'L' or 'H' which corresponds to the low- (1.57 cords/cm) or high-density (3.14 cords/cm) UHTSS textiles, respectively. 'Q' refers to the jacket configuration ('U' and 'W' for U-shaped and fully wrapped jackets, respectively) and 'in' to the number of layers ('1', '2', and '3' for 1, 2 and 3 layers, respectively). For example, B-GH-U2 is a beam with $a/d = 3.5$ strengthened with two-layered U-shaped SRG jackets of 3.14 cords/cm density textile.

The comparison of shear strengthening performance among different systems can rely on their axial stiffness which is defined as [12,13,33,46–49]:

$$S_f = \rho_f E_f \tag{1}$$

where ρ_f ($= 2nt_f w_f / b_w s_f$) is the fibre reinforcement ratio; n is the number of textile layers applied; t_f is the thickness of the textile; w_f is the width of FRCM strips; and s_f is the longitudinal distance of FRCM strips; b_w is the width of the cross-section; and E_f is the elastic modulus of the textile.

As shown in Table 1, all SRG and SRP systems, whether high or low density UHTSS textiles were used, had almost identical axial stiffness, allowing direct comparison between them. In addition, the two-layered CFRCM exhibited lower S_f than SRGs, whereas in case of the three-layered CFRCM is higher.

2.2. Material properties

The specimens were all cast using the same concrete grade. To determine the concrete compressive strength, three 150 mm concrete cubes were tested on the day of beam testing, and the average value was

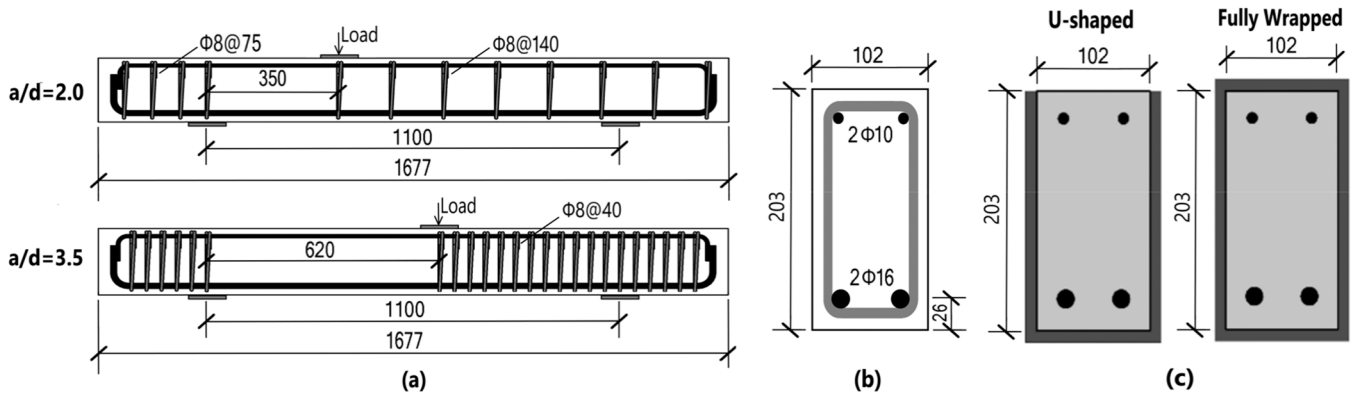

Fig. 1. (a) Layout of the reinforcement; (b) Cross section; (c) Jacket configurations.

Table 1
Specimen details.

Specimens	f_c (MPa)	Strengthening System	Strengthening Configuration	n	ρ_f (‰)	E_f(GPa)	$S_f = \rho_f E_f$ (MPa)
Series A ($a/d = 2.0$)							
A-N	26.4	Control beam	-	-	-	-	-
A-GL-U2	26.7	SRG	U	2	3.29	190	625.10
A-GL-W2	26.6	SRG	W	2	3.29	190	625.10
A-GH-U1	28.5	SRG	U	1	3.31	190	628.90
A-GH-W1	27.3	SRG	W	1	3.31	190	628.90
A-PH-U1	28.2	SRP	U	1	3.31	190	628.90
A-PH-W1	25.7	SRP	W	1	3.31	190	628.90
A-C-U2	29.4	CFRCM	U	2	1.88	252	473.76
A-C-W2	30.5	CFRCM	W	2	1.88	252	473.76
A-C-U3	33.3	CFRCM	U	3	2.82	252	710.64
A-C-W3	32.0	CFRCM	W	3	2.82	252	710.64
Series B ($a/d = 3.5$)							
B-N	24.2	Control beam	-	-	-	-	-
B-GL-U2	24.7	SRG	U	2	3.29	190	625.10
B-GH-U1	26.3	SRG	U	1	3.31	190	628.90
B-PH-U1	25.0	SRP	U	1	3.31	190	628.90
B-C-U2	26.0	CFRCM	U	2	1.88	252	473.76
B-C-U3	25.9	CFRCM	U	3	2.82	252	710.64

Note: f_c = concrete compressive strength on the test day; n = number of textile layers; ρ_f = fibre reinforcement ratio, $2nt_f w_f / b_w s_f$; t_f = textile thickness; w_f is the width of FRCM strips; $s_f$is the longitudinal distance of FRCM strips; E_f = elastic modulus of bare fibres; $\rho_f E_f$ = axial stiffness of strengthening systems.

taken. The concrete compressive strength testing was conducted in accordance with BS EN 12390–3:2019 [50]. Table 1 presents the concrete compression strength for each specimen. In the beams, the yield stresses for the 16 mm- and 10 mm-diameter longitudinal bars were 538 MPa and 527 MPa, respectively. Additionally, the yield stress of the 8 mm-diameter stirrups was measured at 340 MPa. The tensile strength of the steel reinforcement was determined based on ISO 15630–1:2019 [51] and ISO 6892–1:2019 [52].

The same inorganic binder was used in both SRG and FRCM systems which comprised an eco-friendly mineral geo-mortar with a crystalline reaction geo-binder base that only needs to be mixed with water (water-cement ratio 1:5) for use. Its 28-day average bending strength, compressive strength, and bond strength measured according to EN 196–1 [53], EN 12190 [50], and EN 1542 [54], respectively, were reported by the manufacturer to be 8 MPa, 5 MPa, and 2 MPa.

Galvanised unidirectional Ultra-high-tensile-strength steel (UHTSS) textiles were used which comprised high strength steel 3 × 2 cords attached to a fibreglass micromesh for easy installation. The fibreglass

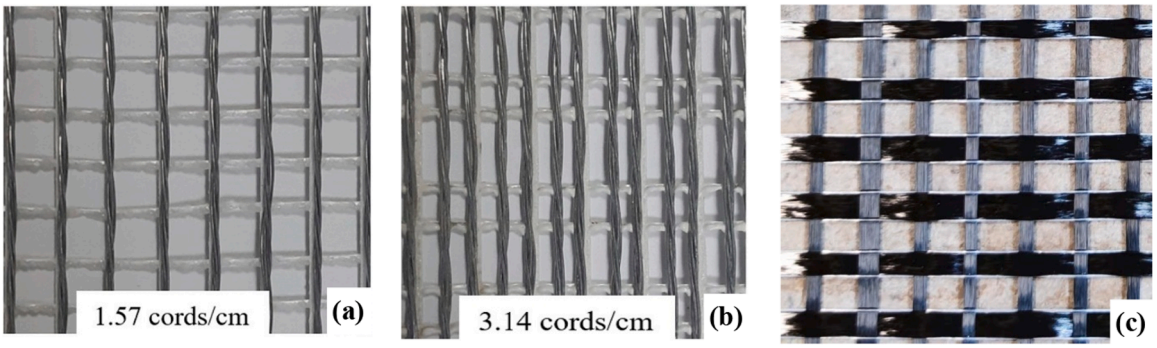

Fig. 2. The three types of textiles used in this study: (a) low-density UHTSS textile; (b) high-density UHTSS textile; (c) carbon textile.

micromesh held the cords in place without adding strength to the composite system [12]. Each cord was made by five twisted wires, among which two filaments wrapped three straight filaments at a high twist angle (see Fig. 2). The geometric and mechanical properties of a single cord are shown in Table 2 as provided by the manufacturer. This experimental study explored two different densities of 1.57 and 3.14 cords/cm, and the equivalent thicknesses per unit width of a single-layer steel fabric, t_f, were 0.084 mm and 0.169 mm respectively (see Table 2). The spacing between successive cords (i.e. density of the textile) is considered a key design parameter for the successful application of the SRG system, since it controls the flow of the cementitious grout through the steel textile and thus determines the quality of the bond between the textile and the matrix. The density should be such as to allow uninhibited flow of the cementitious grout through the steel textile. In case of the SRP systems, the matrix used was a high wettability epoxy mineral adhesive, consisting of two parts mixed in a ratio of 1:3. (Table 3). The carbon textile used in the CFRCM system was a square grid made of high-strength carbon fibre with a mesh size of 10 × 10 mm and an equivalent thickness of 0.048 mm. The mechanical properties of the carbon textile utilised are presented in Table 2. According to the manufacturer, the compressive strength of the mortar was tested based on EN 12190 [55], and the tensile properties of the fabric were tested based on EN 2561 [56].

2.3. Strengthening procedure

Except for the control beams, the rest of the beams were strengthened in the shear critical region (Fig. 1a). Fig. 3 presents the basic steps of the SRG jacketing application. The application procedure for the SRP and SRG/FRCM jacketing systems was similar, except for the critical region preparation step. In the case of SRG/FRCM application, the critical region was roughened before jacket installation, whereas this step was not required for SRP jacketing. U-shaped and fully wrapped jackets were applied, whereas the number of textile layers varied from 1 to 3 layers. It should be noted that in the fully wrapped jacket, the fabric was continuous; while in the U-shaped jacket, each layer was applied individually. As shown in Fig. 3(a), UHTSS textiles due to their high stiffness were pre-bent to facilitate the application. The edges of the beam's cross section were not rounded; hence the textile was bent at right angles [12]. Regarding the FRCM system, the surface of the beam was roughened, cleaned, and saturated with water prior to mortar application (Fig. 3b). The mortar matrix was applied manually with a trowel directly onto the lateral surface of the specimens. Then, the textile was placed immediately after the application of the mortar. The mortar was squeezed out between the steel fibres by applying pressure manually. After applying the first layer of textile, the next layers were applied following the same procedure. To strengthen the beams, each layer of mortar was applied with a thickness of 3–5mm, while the resin layer was applied with a thickness of approximately 1 mm. In case of FRCM and SRG applications, the strengthened area was wrapped with plastic film for curing.

2.4. Test setup & experimental methodology

All beams were subjected to monotonic three-point loading using a stiff steel reaction frame. As shown in Fig. 4, the rectangular beams employed a vertically positioned servo-hydraulic actuator with a capacity of 500 kN, and the load was applied at a displacement rate of 0.02 mm/s. The beams were placed on two steel supports secured to a solid floor with threaded rods, which were subjected to monotonically increasing external loads until failure. An external LVDT (Linear Variable Differential Transducer) was used to measure the vertical displacement of the beam at the load application position. The remaining two LVDTs were employed to monitor the settlement at the supports. Additionally, Digital Image Correlation (DIC) technology was used to capture the strain contours of the tested beams. The shear critical region of each beam was painted with a speckle pattern using a special brush and black ink. A high-performance camera was placed on a distant tripod to collect the displacement changes of the relevant area at the rate of one photo every two seconds. Finally, a DIC software was used to post process the high-resolution speckle images.

Table 3
Properties of the mortars and resin.

	Mixture Density (kg/cm^3)	f_{cm} (MPa)	f_f (MPa)	f_b (MPa)	E_f (GPa)
Mortar	2050	50	8	2	22
Resin	1600	-	-	14	5.3

f_{cm} = compressive strength (28 d); f_f = flexural strength (28 d); f_b = bond strength (28 d).

3. Experimental results and discussion

Table 4 summarizes the test results such as the peak load ($P_{\max}$) and the corresponding displacement ($\delta_{\max}$); the strength increase of the retrofitted beams ($\Delta P_{\max} = P_{RET} - P_{CON}$; where P_{RET} and P_{CON} are the peak load of the retrofitted and the corresponding control beam); the ultimate load P_u= (80 %$P_{\max}$) and the corresponding displacement δ_u; the shear strength of the critical shear span (V; for the control specimen it is equal to V_{CON}; for the retrofitted specimens it is equal to V_{RET}); the shear strength provided by the strengthening system V_{JAC}(= $V_{RET} - V_{CON}$; where V_{RET} and V_{CON} are the shear strength of the retrofitted and the corresponding control beam); energy absorption, Ψ; and the failure mode. When a descending branch in the load-deflection curve is not present, the ultimate deflection is the last point on the curve, denoted as δ_u.

In general, the experimental results demonstrated that the SRG, SRP and CFRCM systems can improve the shear capacity of RC beams. Additionally, as a/d increased, the shear strength of the jacketed beams (V_{RET}) decreased but the shear strength provided by the strengthening system across all strengthening systems (V_{JAC}/V_{RET}) was increased. The reduction in V_{JAC} can be attributed to three factors. As the beam transitions from deep to slender, the carrying mechanism shifts from arch action to a truss-like system, inherently decreasing the absolute shear resistance [21,32]. In addition, the larger shear span increases the likelihood of shear damage, impairing the bond between the jacket and substrate, facilitating detachment [27]. The higher a/d ratio induces pronounced shear concentration around beam ends [57,58], contributing to premature failure of the strengthening system and diminished shear enhancement, as evidenced by the DIC strain fields of Series B

Table 2
Properties of the textiles.

	t_f (mm)	Weight (g/m^2)	A (mm^2)	Density (Cords/cm)	f_{fu} (MPa)	E_f (GPa)	ε_{fu} (%)
Steel-High density (3.14 cords/cm)	0.084	670	0.538	1.57	3000	190	1.5
Steel-Low density (1.57 cords/cm)	0.169	1200	0.538	3.14	3000	190	1.5
Carbon (10mm×10 mm)	0.048	170	-	-	-	252	2.0

A = cord area; f_{fu} = tensile strength; ε_{fu} = fibre's strain to failure.

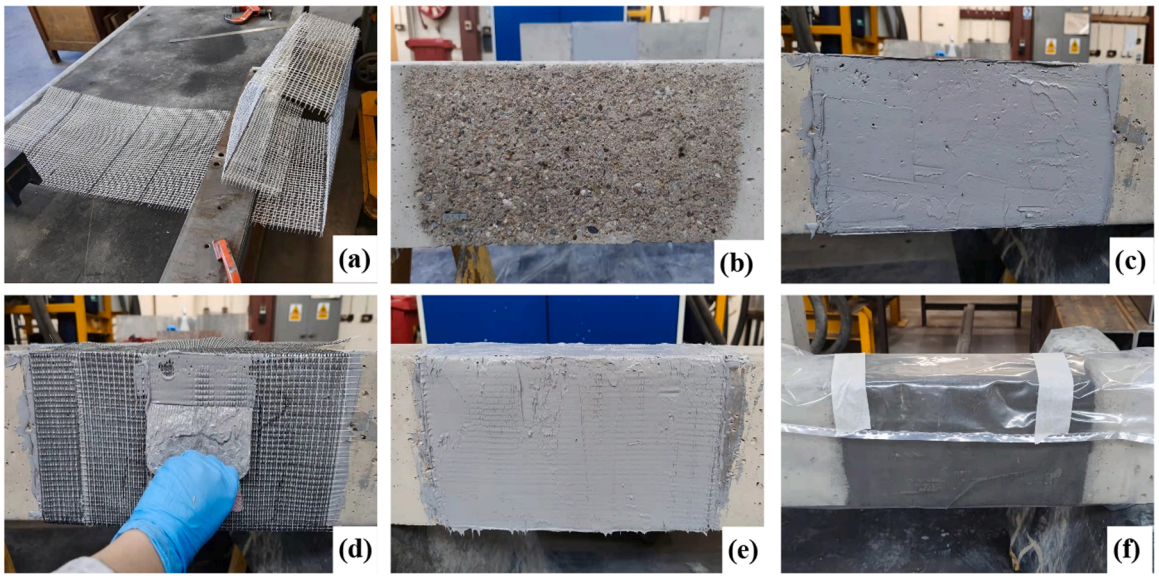

Fig. 3. Steps of the SRG jacketing application: (a) pre-bending the textile; (b) roughening and cleaning the surface in the shear critical zone; (c) applying the first matrix layer; (d) placing the textile; (e) repeating application process until complete; (f) curing the strengthened area.

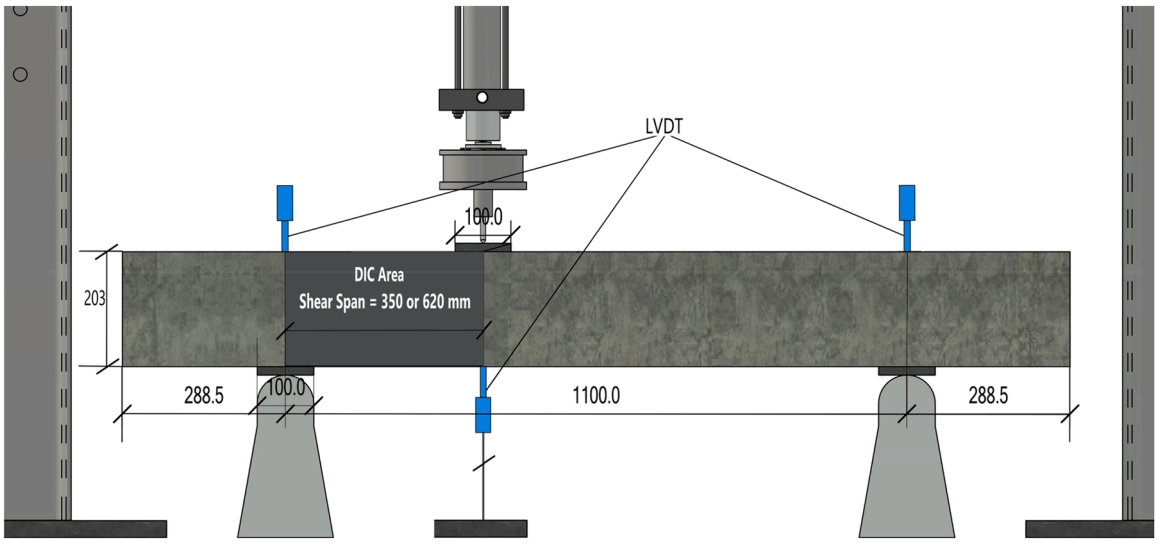

Fig. 4. Test setup, configuration of the DIC at the shear-critical span, and LVDTs positions.

beams in Fig. 8.

The failure modes are also presented in Table 4, where S is the failure caused by diagonal tension, fibre rupture; S-D stands for shear-detachment failure, that is, shear failure occurs when detachment occurs either between the composite and the beam substrate or within the mortar layer; S-F indicates shear-flexural failure, in which the beam exhibits some signs of flexural failure, but eventually shear failure occurs due to sudden detachment of the jacket; and F-R represents flexural-rupture failure where concrete fracture follows the longitudinal steel bar yielding with fibre rupture.

3.1. Failure modes

Series A beams: Fig. 5 illustrates the condition of the A-series beams at the end of testing. The control beam, A-N, experienced diagonal tension failure as shown in Fig. 5(a). A single inclined crack appeared initially, expanding with increasing load, leading to brittle shear failure.

The U-shaped SRG and SRP jacketed beams failed due to shear-detachment prior to flexural yielding (Fig. 5(b, d, f)). As the load increased, vertical cracks appeared at the bottom of the beam, followed by rapid deflection and eventual sudden detachment of the jacket, resulting in failure. Various failure modes were observed; A-GL-U2 experienced jacket detachment and slippage of the textile fibres, while A-GH-U1 displayed poor adhesion, leading to detachment between the textile and mortar. In contrast, the resin matrix in A-PH-U1 exhibited better adhesion, leading to the peeling of the concrete cover layer. This is because the mortar as a coarse matrix cannot penetrate the overly fine gaps of high-density fabrics, while the resin as a finer matrix can more effectively pass through these gaps and bond with the textile.

The fully wrapped SRG and SRP beams (A-GL-W2, A-GH-W1, A-PH-W1, Fig. 5(c, e, g)) displayed a ductile behaviour compared to the U-shaped jacketed beams. Flexural cracks formed, gradually widening until reaching the yielding point, with the SRG or SRP system allowing ongoing deformation. Specifically, A-GL-W2 and A-PH-W1 failed by fibre rupture after yielding of steel, while A-GH-W1 experienced sudden detachment of the jacket leading to shear failure.

Table 4
Summary of test results.

Series	Beam	P_{max} (kN)	ΔP_{max} (%)	P_u (kN)	δ_{max} (mm)	δ_u (mm)	$V = V_{RET}$ (kN)	V_{JAC} (kN)	V_{JAC}/V_{RET} (%)	$\Psi = \Psi_{RET}$ (kN·mm)	Failure Mode
A	A-N	51.3	-	41.1	2.50	3.96	35.0*	-	-	87.1**	S
	A-GL-U2	109.8	114	87.9	3.53	5.33	74.9	39.9	53.3	214.5	S-D
	A-GH-U1	97.5	90	78.0	3.15	3.95	66.5	31.5	47.4	172.3	S-D
	A-GL-W2	114.8	124	108.7	24.32	30.8	78.3	43.3	55.3	2636.9	F-R
	A-GH-W1	107.7	110	85.6	9.51	9.73	73.4	38.5	52.5	773.7	S-F
	A-PH-U1	112.5	119	90.0	3.89	4.33	76.7	41.7	54.4	250.6	S-D
	A-PH-W1	141.5	176	113.2	17.70	31.6	96.5	61.5	63.7	3831.0	F-R
	A-C-U2	106.7	107	85.3	3.96	4.42	72.8	37.8	51.9	268.1	S-D
	A-C-U3	120.2	134	96.1	4.42	4.87	82.0	47.0	57.3	323.6	S-D
	A-C-W2	133.8	161	107.1	5.76	6.41	91.2	56.3	61.7	471.6	S-D
	A-C-W3	140.6	174	112.5	7.30	7.41	95.9	60.9	63.5	561.2	S-D
B	B-N	38.8	-	31.1	1.41	1.50	16.9*	-	-	31.5**	S
	B-GL-U2	102.6	164	82.1	4.70	7.30	44.8	27.8	62.1	272.7	S-D
	B-GH-U1	105.0	170	84.0	5.17	6.74	45.8	28.9	63.1	309.8	S-D
	B-PH-U1	120.9	211	96.7	5.98	6.23	52.8	35.8	67.8	403.2	S-D
	B-C-U2	117.9	204	94.3	5.82	6.70	51.4	34.5	67.1	385.0	S-D
	B-C-U3	122.4	215	97.9	5.62	6.36	53.4	36.5	68.4	373.0	S-D

* $V = V_{CON}$ for the control specimen
** $\Psi = \Psi_{CON}$ for the control specimen.

For CFRCM-strengthened beams, both U-shaped and fully wrapped configurations exhibited shear-detachment failure, as depicted in Fig. 5 (h-k). In the case of the two-layered systems (A-C-U2 and A-C-W2), cracks developed near the support and at the load application location as the load increased. Subsequently, the cracks progressed into a diagonal crack that that extended across the entire shear-critical region. The detachment of both the mortar and textile in the crack area ultimately resulted in the failure of the beam. In addition, a three-layer carbon fibre textile was employed to further increase the beam's stiffness and alter the stress transfer mechanism of A-C-U3 and A-C-W3, which eliminated the occurrence of cracks penetrating the entire surface. After detachment failure, the textile remained undamaged upon removing the mortar from the cracks. Interestingly, there was a slight variation in CFRCM system's failure modes when the U-shaped configuration was replaced with the fully wrapped configuration for the same number of layers.

Series B beams: For the Series B beams (shear span-to-depth ratio of 3.5), the control beam B-N failed in a typical diagonal tension mode with sudden shear cracking and formation of large diagonal cracks (Fig. 6(a)). For the strengthened beams (Fig. 6(b-f)), shear failure occurred for all cases with detachment of the jacket from the substrate (including part of the concrete cover layer). The failure modes mirrored those of the corresponding specimens with $a/d = 2.0$. Among the SRG and SRP systems, B-GH-U1 peeled off the least amount of cover layer at failure while B-PH-U1 peeled off the most. This is because the epoxy resin provides higher adhesion compared to the mortar matrix, resulting in larger portions of the concrete cover being peeled off at failure. Regarding the CFRCM systems, no peeling off of the mortar portion from the CFRCM surface was observed for B-C-U3 at failure, while such partial phenomenon occurred for the two-layered CFRCM system (B-C-U2).

To summarise, the potential of closed SRG jackets to modify the response of shear deficient beams from brittle to ductile was demonstrated (i.e. A-GL-W2 and A-PH-W1). Irrespective of the jacketing system applied herein (i.e. SRG, SRP, CFRCM) and the shear-to-span ratio (a/d =2 and 3.5), all beams strengthened with U-shaped jackets failed due to shear-detachment.

3.2. Evolution of damage based on digital image correlation

Series A beams: Fig. 7 shows the horizontal and vertical strain fields of the Series A beams (excluding A-C-U2 due to a technical issue) at peak load, as obtained by Digital Image Correlation (DIC). The control beam A-N displayed pronounced diagonal cracking in both horizontal and vertical directions, in addition to flexural cracks that were not fully developed. All strengthened beams exhibited extensive strain distribution within the critical region compared to the control beam. Notably, A-GL-W2 and A-GH-W1 which failed in flexure showed wider strain distribution, with the jacket preventing the formation of diagonal cracks. However, oblique cracks still formed in U-shaped SRG and SRP jacketed beams. Due to fact that UHTSS textiles comprise unidirectional cords, SRP- and SRG-strengthened beams presented considerable strains only in the horizontal direction, while CFRCM systems displayed larger vertical strains.

Series B beams: Fig. 8 illustrates the horizontal and vertical strain fields observed at peak load for the beams with $a/d = 3.5$, obtained using DIC. The control beam, B-N, showed more incomplete vertical deformations than A-N at peak load. In contrast to Series A beams, Series B strengthened beams exhibited larger areal deformations, primarily on one side near the support. This can be attributed to the altered shear force distribution near the beam ends due to the end restraint effect of the supports. The higher shear span ratio in Series B led to more concentrated shear forces near the supports, causing easier damage in sections adjacent to them. For B-C-U2 and B-C-U3, it can be observed that increasing the number of fabric layers further optimised the stress distribution. The three-layered CFRCM jacketed beam showed smaller deformations at peak load without any mortar peel-off at the surface.

3.3. Load-deflection curves

Fig. 9 depicts the load-deflection responses of the series A beams ($a/d = 2.0$) strengthened by SRG, SRP, and CFRCM jackets. The control beam failed in shear at a peak load of 51.3 kN (corresponding displacement of 2.5 mm). All the U-shaped SRG jacketed beams failed in shear with a strength increase in a range of 90–114 % (Fig. 9a). Regarding the fully wrapped jacketed beams, A-GL-W2 (low-density UHTSS fully wrapped jacketed beam) showed a small drop in strength at 75 kN, which indicated some degree of textile detachment, while the SRG system still contributed to the shear resistance up to the peak load (124 % higher than the control beam). However, A-GH-W1 (high-density UHTSS fully wrapped jacketed beam) failed due to detachment of the jacket (shear-detachment) at a load 110 % higher than the control beam. In case of the U-shaped CFRCM strengthened beams, which all failed in shear, the strength increased by 58 % and 77 % for the two- and three-layered U-wrapped beams (A-C-U2 and A-C-U3), respectively. The fully wrapped A-C-W2 and A-C-W3 beams exhibited higher strength increase of 130 % and 192 %, respectively. Meanwhile, Fig. 9(c) shows

Fig. 5. Crack patterns and failure modes of Series A beams.

that the SRP reinforced beams A-PH-U1 and A-PH-W1 had different results, with A-PH-U1 failing in shear due to jacket detachment, while increasing strength by 119 %. The SRP fully wrapped beam, A-PH-W1, showed a transition from brittle to ductile failure mode, with strength and deflection increasing by 176 % and 608 %, respectively.

Fig. 10(a) and (b) depict the load-deflection responses of the strengthened beams, using identical jacket configurations for $a/d = 2.0$ and 3.5, respectively. In beams with a/d= 2.0 (deep beams), the predominant mechanism governing the shear resistance is that of the arch action, whereas for the beams with a/d= 3.5 (slender beams), the dominant mechanism shifts towards beam action, resembling a truss analogy mechanism. The peak loads of series B strengthened beams (except B-GL-U2) demonstrated a slight increase compared to the Series A beams. This increase is because the slender beams distribute a smaller portion of shear force across the strengthened region under the same load, thereby delaying shear failures to some extent. Furthermore, the strengthened beams in Series B exhibited substantially larger deflections and lower stiffness compared to Series A beams due to increased moments associated with the higher a/d [32] (Table 4).

3.4. Energy absorption

The energy absorption (Ψ) of the strengthened beams was defined as the area under the load-displacement curve of the beam up to the point of failure [14,17,59]. For beams that failed in shear, the Ψ value was calculated up to the peak load, while for beams with ductile performance (i.e. flexural failure), Ψ was calculated up to the ultimate point (80 % of the peak load). The Ψ results for all tested beams are presented in Table 4. Additionally, the relationship between the energy absorbed by the jacket (Ψ_{JAC}) (i.e. difference between the energy absorption of the strengthened beam (Ψ_{RET}) and that of the control beam (Ψ_{CON})), and the beam's textile axial stiffness ($\rho_f E_f$) is presented in Fig. 11.

With an increase in the a/d ratio, the B series strengthening systems exhibited greater energy absorption compared to the A series. Notably, for beams failing in a ductile mode (such as A-GL-W2 and A-PH-W1), the Ψ_{JAC} values surpassed those associated with beams failing due to shear-detachment. In comparison to the control A-N, the energy absorption of these beams increased by up to 4298 %. This indicates that fully wrapped SRG and SRP jackets can significantly enhance the resilience of shear-deficient RC beams. Moreover, no significant differences were

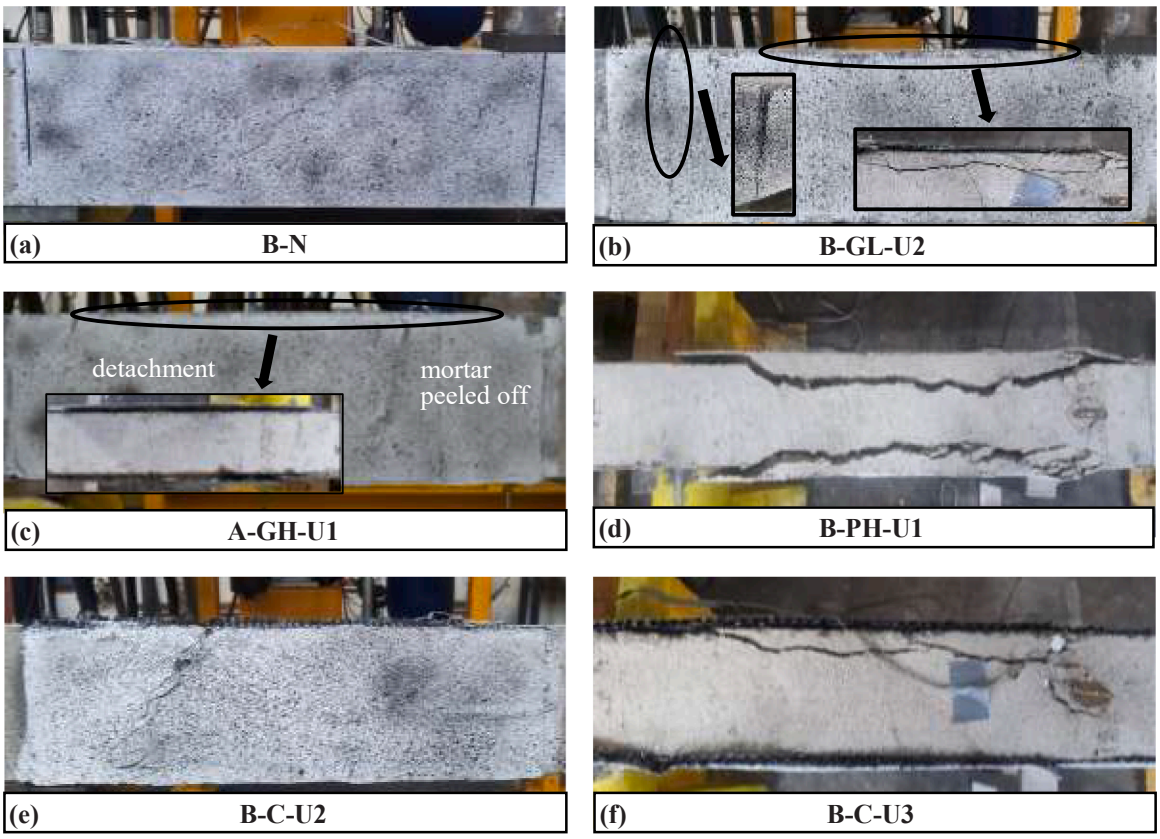

Fig. 6. Crack patterns and failure modes of Series B beams.

observed between the U-shaped SRP and SRG systems, irrespective of whether they belonged to the A or B series. Additionally, the energy absorption of CFRCM showed a proportional increase with the axial stiffness of the fabric. Both fully wrapped and U-shaped configurations displayed a consistent linear increase in slope, aligning with previous findings [7]. In summary, the fully wrapped SRP and low-density SRG systems, particularly SRP, exhibited remarkable ductility, suggesting their potential effectiveness in reinforcing structures to withstand seismic and other high-intensity loads in practical engineering applications.

3.5. Parameters affecting the performance of the strengthened beams

3.5.1. Effect of the shear span-to-depth ratio

Fig. 12 depicts the impact of a/d on the enhancement of shear strength (V_{JAC}/V_{CON}) for all jacketed beams. As observed, V_{JAC}/V_{CON} increases as a/d increases. The strength increase in the B-PH-U1 surpasses that of A-PH-U1 by 102 %. The smallest increment is observed in the two-layer low-density SRG system (B-GL-U2 vs A-GL-U2), albeit still reaching 50 %. For Series A beams (a/d=*2,* deep beams), after the formation of diagonal cracks, arch action predominates. The majority of the load is directly transferred from the load application point to the support through diagonal compressed struts, meaning the load is primarily carried by diagonal compressed struts [32]. The influence of arch action diminishes with the increase in the a/d ratio, reducing the concrete's contribution to shear strength. However, this is offset by an increase in the contribution of the strengthening system acting as lateral reinforcement on the beam [32,60]. Moreover, for deep beams, inclined cracks are oriented more obliquely relative to the fibre alignment (vertical direction) of the fabrics. Hence, stresses along the fibre orientation are less effective in impeding crack propagation and widening. With increasing shear span-depth ratio, the angle between the fibres and crack opening direction is reduced, decreasing the proportion of shear force undertaken horizontally by the fabrics, which thereby elevates the percentage of shear contribution provided by the strengthening system [41].

3.5.2. UHTSS: effect of the textile density and the matrix type

The impact of the UHTSS density on V_{JAC}/V_{CON} of beams strengthened with UHTSS textiles' systems is shown in Fig. 13(a). In Series A beams, the V_{JAC}/V_{CON} of the low-density U-shaped SRG jacketed beam (A-GL-U2) was 24 % higher than that of the high-density counterpart (A-GH-U1), while the fully wrapped low-density SRG exhibited a 14 % higher shear strength. These findings suggest that a UHTSS density of 3.14 cords/cm obstructed the passage of mortar, resulting in reduced adhesion of the textile to the matrix and poor strengthening performance. This low adhesion also caused debonding at the interface between the textile and matrix, as well as delamination of the internal mortar layer, leading to decreased composite integrity and premature detachment of jackets [31,32]. However, both B-GL-U2 and B-GH-U1 highlighted nearly identical shear strength enhancement. The deficient performance of B-GL-U2 may be attributed to defects in the strengthening application. Hence, it can be concluded that in case of the SRG strengthening system, the use of high-density (>3.14 cords/in) UHTSS textiles results in poor adhesion. This is in agreement with previous research where it was concluded that due to the small gaps between the cords in case of the 4.72 cords/cm density UHTSS textiles imposed difficulties in the penetration of the mortar [7]. Thus, it is recommended to use a UHTSS textile density of less than 3.14 cords/cm (4 cords/in) for optimal results in the SRG system.

With respect to the matrix influence on high-density UHTSS systems (Fig. 13b), the resin-based system (SRPs) showed greater shear strength enhancement than the mortar-based system (SRGs), irrespective of the series. This implies that the fine resin substrate could impregnate the gaps in the high-density UHTSS textiles more effectively than the coarser mortar, thereby providing superior adhesion.

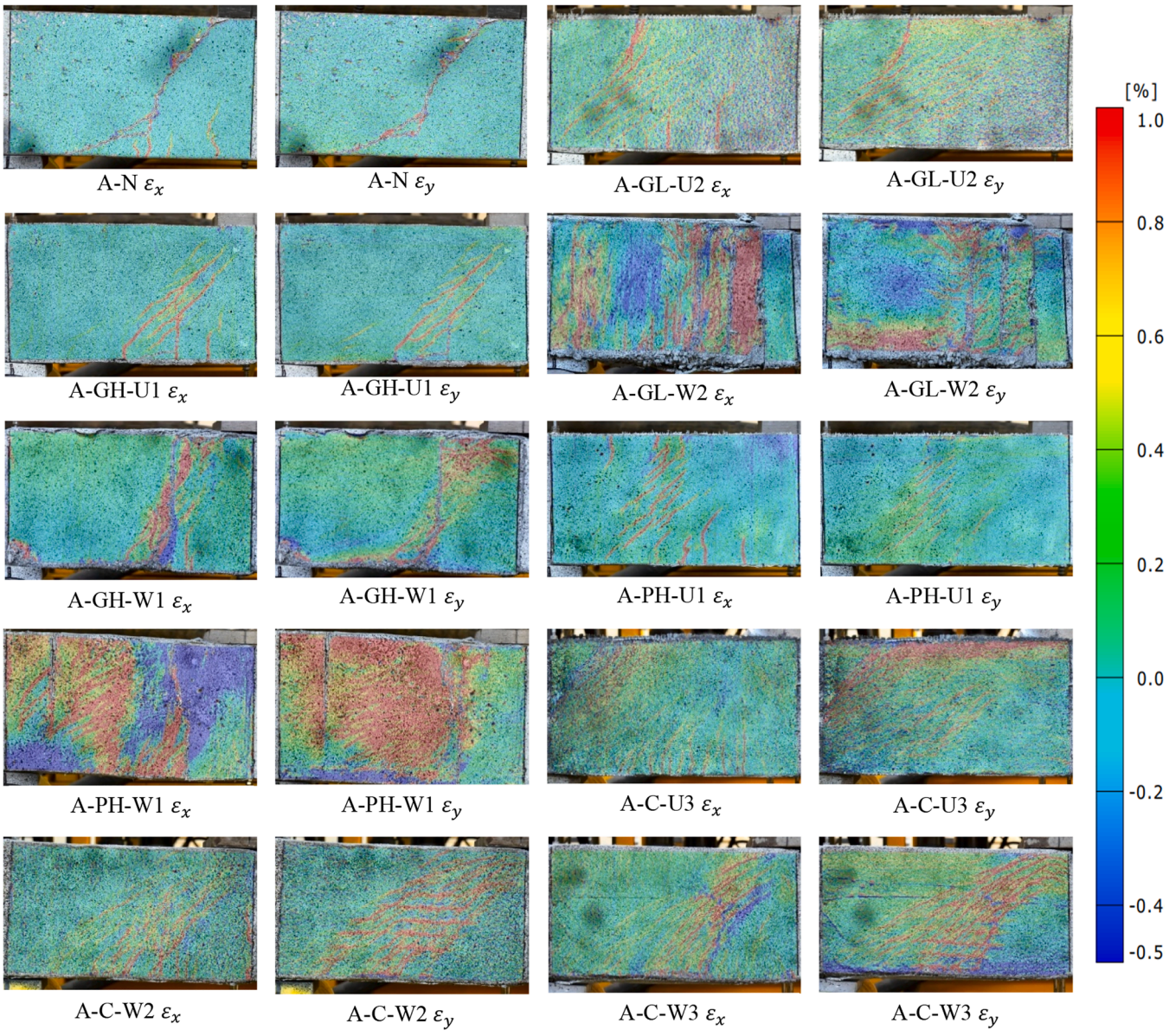

Fig. 7. Strain contours in the critical shear span for series A beams at peak load.

3.5.3. Effect of the fibre type and number of layers of textile

To assess the impact of different fibre types and the number of textile layers, Fig. 14 illustrates the V_{JAC}/V_{CON} of varied CFRCM and SRG in A series, grouped based on distinct strengthening configurations. Among the tested setups, A-C-W3 demonstrated the most significant improvement in shear strength, reaching up to 174 %, while A-GH-U1 exhibited the least favorable result at only 90 %. Despite the lower axial stiffness of the two-layered CFRCM compared to SRG, it can still achieve similar or even superior shear strength enhancement. However, Fig. 10(b) indicates that the CFRCM system lacks the ability of the SRG jacket to induce a ductile failure mode in the beam. Additionally, the three-layer CFRCM, designed to mitigate shear failure, still manifested shear-detachment failure. Concerning the impact of the number of layers, two- and three-layered U-wrapped beams demonstrated strength increases of 58 % and 77 %, respectively. In contrast, fully wrapped beams with two- and three-layered CFRCM jackets exhibited even higher strength increases, at 130 % and 192 %, respectively. Therefore, an increase in the number of textile layers contributes to enhancing the shear strengthening effectiveness of the FRCM system.

4. Prediction of the shear strength of SRG-jacketed beams

The shear span-to-depth ratio (a/d) has a significant impact on the shear strength of RC beams. However, existing models rarely consider the influence of shear span-to-depth ratio, especially in the case of SRG jacketing. Wakjira and Ebead [32] developed a model to predict the shear strength of U-shaped jacketed SRG beams considering the effect of a/d. This model, however, does not account for side bonding, full wrapping, and fibre rupture failure. Additionally, Wakjira and Ebead's model [32] requires the knowledge of the longitudinal reinforcement strains, which may impose challenges in the implementation of the model.

Therefore, a model is developed to predict the shear strength of SRG-strengthened beams with no transverse reinforcement. This model could also be applied in cases of sparsely spaced and corroded links, considering that the contribution of the internal transverse reinforcement is negligible. To develop and validate the model, an experimental database was compiled using experimental results from this study and existing literature [12,31,32,34]. The strengthened beams included in the database did not have any anchoring mechanisms anchoring

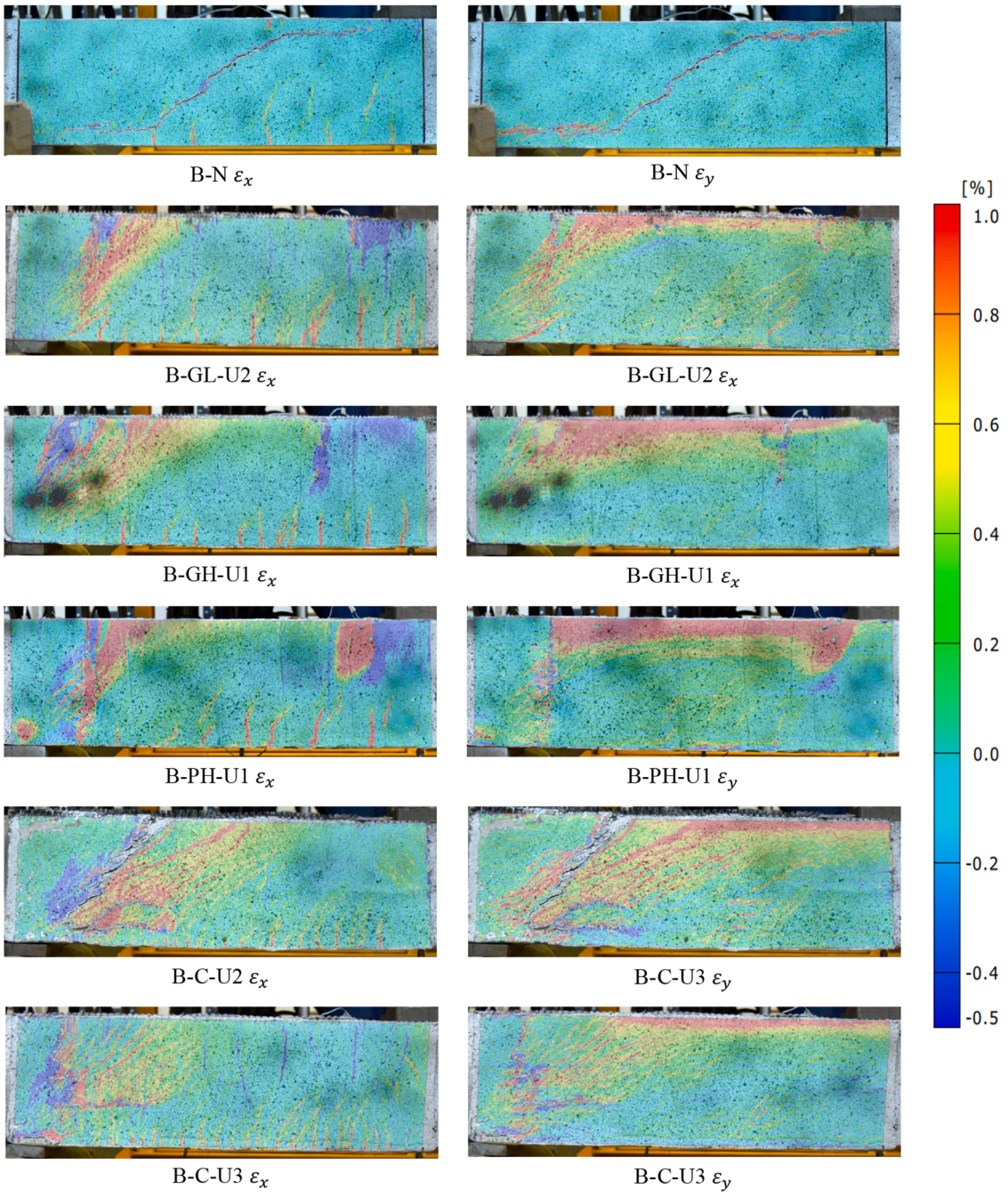

Fig. 8. Strain contours in the critical shear span for series B beams at peak load.

mechanisms and transverse reinforcement, and all experienced shear failure.

Table 1 presents the main mechanical properties, experimental results, and predicted results of 25 SRG-strengthened beams in the database. The model uses Eurocode 2 to calculate the shear strength provided by the concrete beam (V_c) and estimates the shear strength provided by the SRG (V_{JAC}) based on the model of Chen & Teng [19]. The shear span-to-depth impact factors R_c and R_f for V_c and V_{JAC}, respectively, were introduced through Wakjira and Ebead's model [32]. This model eliminates the need for longitudinal steel strain in calculations, and incorporates side bonding, full wrapping, and fibre rupture failure of SRG jackets. The shear strength of the strengthened beams (V) can be calculated as:

$$V = R_c V_c + R_f V_{JAC} \tag{2}$$

According to [12,33,34], the shear strength contributed by the concrete beam is typically calculated using the model in EC2 [61]:

$$V_C^{EC2} = 0.18k\left(100\rho_{long} f_c'\right)^{1/3} b_w d \tag{3}$$

where, f_c' is the compressive strength of concrete obtained from cylinders; d is the depth of the cross-section; ρ_{long} is the area ratio of the tensile reinforcement; and $k = 1 + \sqrt{(200/d)} \leq 2.0$ (with d in mm) is a factor that considers the size effect.

The shear strength of SRG jackets (V_{JAC}) is calculated by the model proposed by Chen & Teng [62,63]. This model initially developed for FRP systems, but existing research [32,64,65] has demonstrated its applicability to FRCM systems. The V_{JAC} can be calculated as:

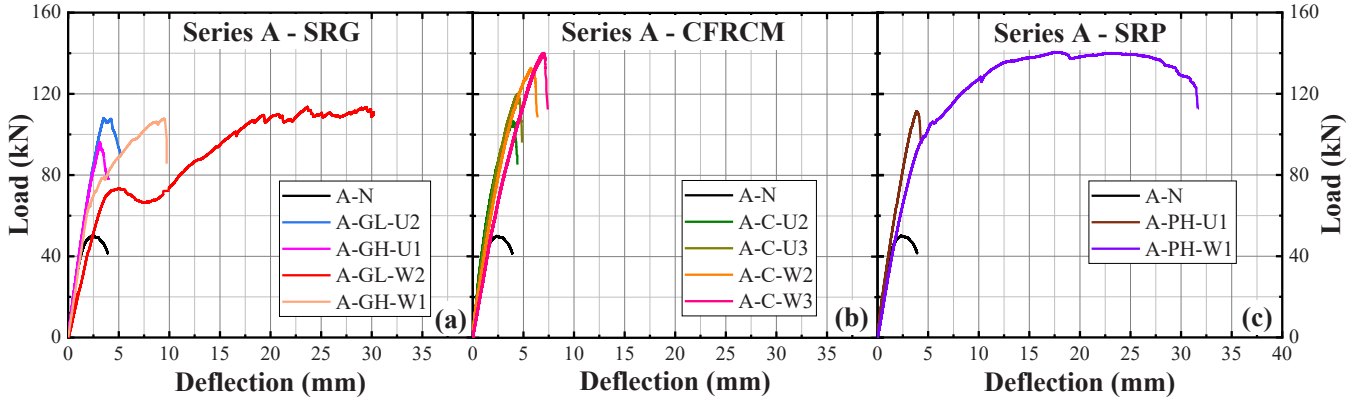

Fig. 9. Load-deflection curves for all tested specimens with a/d= *2* (Series A beams): (a) SRG; (b) CFRCM; (c) SRP strengthened beams.

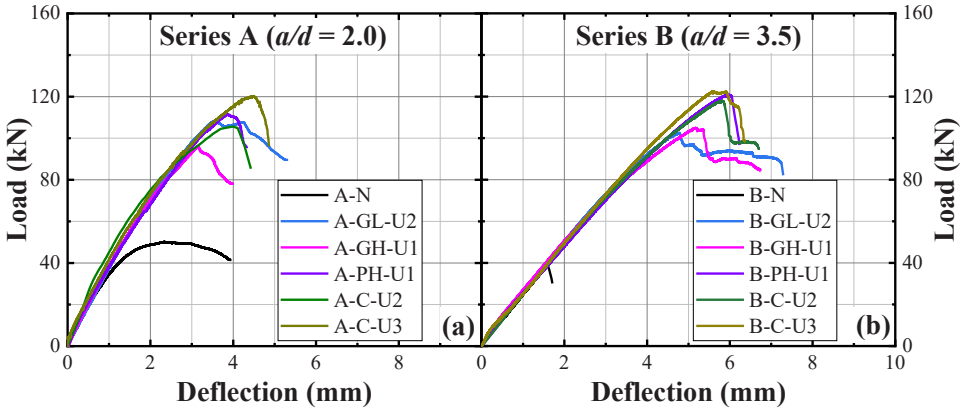

Fig. 10. Effect of a/d on the load–deflection response of beams: (a) Series A (a/d = 2.0); (b) Series B (a/d = 3.5).

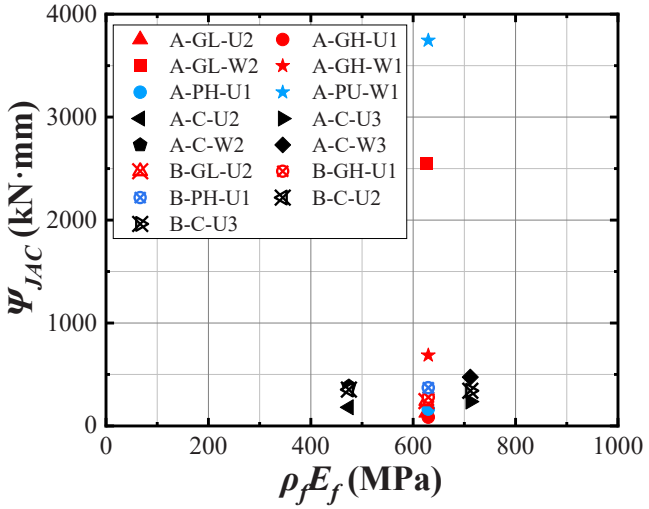

Fig. 11. Energy absorption vs axial stiffness for the strengthened beams.

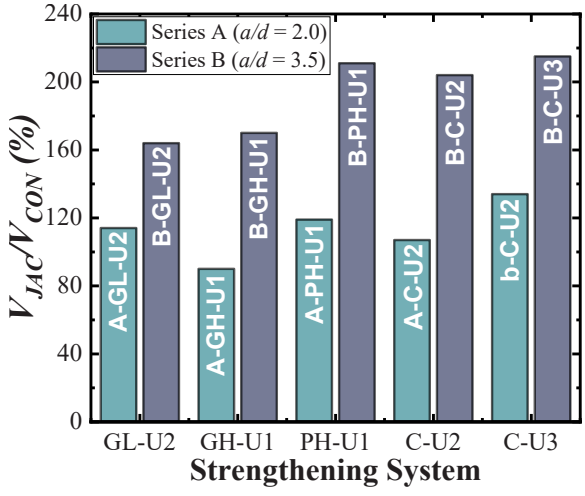

Fig. 12. Effect of the a/d ratio on V_{JAC}/V_{CON}.

$$V_{JAC} = 2nt_f b_w h_{fe} \frac{w_f}{s_f} f_{fed}(\cot\theta \sin\alpha + \cos\alpha) \quad (4)$$

whereα is the angle between the fibres and the beam axis perpendicular to the shear force, taken as 90°; θ is the angle of the critical shear cracks to x-axis, taken as 45°. f_{fed} is the effective stress of SRG at failure; h_{fe} is effective hight of SRG, $= z_b - z_t$; $z_b = 0.9d - (h - d_{fb})$; $z_t = d_{ft}$, in which z_b and z_t are the co-ordinates of the top and bottom ends of the effective FRCM; d_{fb} is the distance from the compression face to the top edge of the FRCM; and d_{ft} is the distance from the compression face to the lower edge of the jacket.

The effective stress of SRG is given by [62,63,65]:

$$f_{fed} = D_f f_{fed,\max} \le f_{fu} \quad (5)$$

where D_f is the stress distribution coefficient; and $f_{fed,\max}$ is the maximum design stress of the jackets.

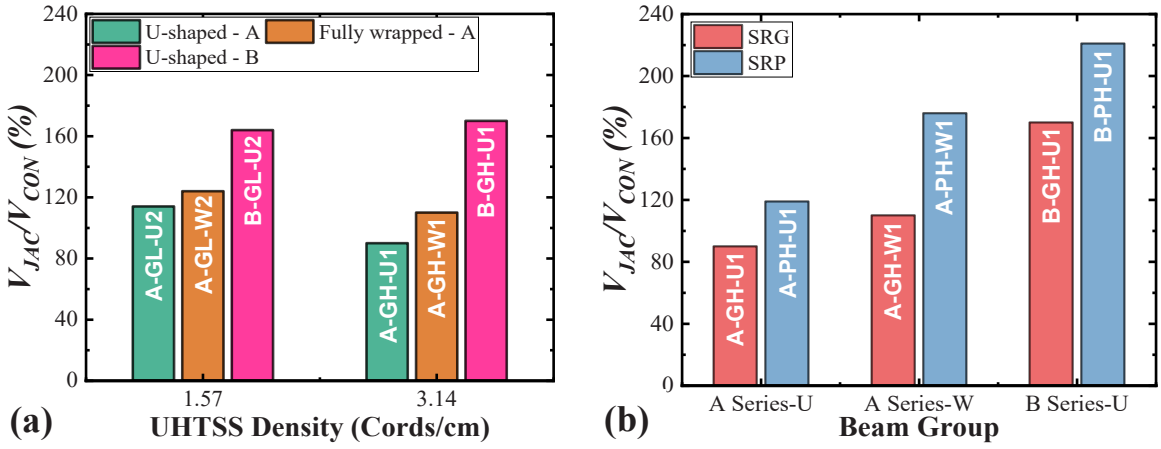

Fig. 13. Effect of the UHTSS textile density and the system matrix.

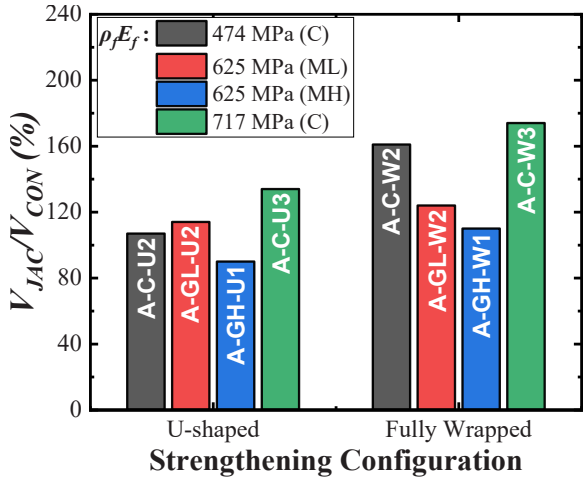

Fig. 14. Effect of the fibre type and layers of textile.

Regarding the SRG strengthened beams with detachment failure [63], the maximum design stress of the SRG is calculated as:

$$f_{fed,\max} = 0.427\beta_l\beta_w\sqrt{\frac{E_f\sqrt{f_c'}}{nt_f}} \tag{6}$$

The effective bond length and the concrete width ratio of the jacket, β_l and β_w are given as

$$\beta_l = \begin{cases} 1, \lambda \geq 1 \\ \sin\left(\frac{\pi\lambda}{2}\right), \lambda < 1 \end{cases} \tag{7}$$

$$\beta_w = \sqrt{\frac{2 - w_f/(s_f\sin\alpha)}{1 + w_f/(s_f\sin\alpha)}} \tag{8}$$

where λ is the maximum bond length parameter, given by:

$$\lambda = L_{\max}/L_e \tag{9}$$

where $L_{\max}$ and L_e are the available bond length and the effective bond length, respectively, given by the following:

$$L_{\max} = \begin{cases} h_f/\sin\alpha, & \text{for U} - \text{shaped jackets} \\ h_f/2\sin\alpha, & \text{for side bonding jackets} \end{cases} \tag{10}$$

$$L_e = \sqrt{\frac{E_f n t_f}{\sqrt{f_c'}}} \tag{11}$$

The expression of the stress distribution coefficient (D_f) for side bonding and U-shaped jackets is:

$$D_f = \begin{cases} \frac{2}{\pi\lambda}\left(\frac{1-\cos\left(\frac{\pi\lambda}{2}\right)}{\sin\left(\frac{\pi\lambda}{2}\right)}\right), \lambda \leq 1 \\ 1 - \frac{\pi - 2}{\pi\lambda}, \lambda > 1 \end{cases} \tag{12}$$

According to [62], the expression of the stress distribution coefficient (D_f) for fully wrapped jackets is:

$$D_f = \frac{1 + z_t/z_b}{2} \tag{13}$$

Regarding the SRG strengthened beam with fibre rupture failure, the maximum design stress of the SRG is calculated as:

$$f_{fed,\max} = f_{fu,jac} \tag{14}$$

where $f_{fu,JAC}$ is the ultimate stress of jackets. It is worth noting that Eq. (14) was originally proposed for only fully wrapped jackets exhibiting the fibre rupture failure mode [66]. However, recent studies [33,65] have reported the possibility for U-shaped jackets also experiencing this failure mode. Therefore, this study endeavours to extend its applicability to both fully wrapped and U-shaped jackets. Considering the limitation of the data, further validation is necessary to confirm its effectiveness. According to [67,68], the strength of FRCM can be calculated by the following formula when jacket debonding failure does not occur:

$$f_{fu,JAC} = E_f\varepsilon_{fe,jac} \leq f_{fu,f} \tag{15}$$

where $\varepsilon_{fe,jac}$ represents the effective strain of FRCM, considering only the fibres distributed along the main direction of the textile (Vertical); and $f_{fu,f}$ is ultimate stress of fibres. According to the strengthening configuration, $\varepsilon_{fe,jac}$ can be calculated as [67]:

$$\varepsilon_{fe,jac} = \begin{cases} 0.035\left(\frac{f_c'^{2/3}}{\rho_f E_f}\right)^{0.65}\varepsilon_{fu,f}, & \text{for fully wrapped jackets} \\ 0.020\left(\frac{f_c'^{\frac{2}{3}}}{\rho_f E_f}\right)^{0.55}\varepsilon_{fu,f}, & \text{for U} - \text{shaped jackets} \end{cases} \tag{16}$$

In Eq. (16), E_f and f_c' are expressed in GPa and MPa, respectively. $\varepsilon_{fu,f}$ is the ultimate strain of fibres.

Substituting Eq. (3) and Eq. (4) into Eq. (2), the final expression for the shear strength of the strengthened beam is obtained:

$$V = R_c V_c + R_f V_{JAC} = R_c 0.12k\left(100\rho_{long} f_c'\right)^{1/3} b_w d + R_f 2nt_f b_w h_{fe} f_{fed} \quad (17)$$

Based on regression analysis of the data, the influence factors of a/d on the beam and SRG jacket (R_c and R_f) are:

$$R_c = \begin{cases} (2.47/\chi)^{\eta}, & a/d \le 2.5 \\ 0.86\eta^{1.25}, & a/d > 2.5 \end{cases} \quad (18)$$

$$R_f = \begin{cases} 1.39\sqrt{R_c}, & a/d \le 2.5 \\ 0.7R_c^{3/4}, & a/d > 2.5 \end{cases} \quad (19)$$

Where $\chi = a/d$, $\eta = 2.5/\chi$.

Table 5 presents the shear strength of SRG-strengthened beams obtained using the proposed model, and the ratio of predicted to experimental results (V_{pred}/V_{exp}). A comparison between experimental and predicted shear strengths is illustrated in Fig. 15. The results indicate that the proposed model accurately predicts the shear capacity, and the predicted values are conservative in most cases. The average and standard deviation (STD) of V_{pred}/V_{exp} are 0.99 and 0.15, respectively, with a correlation coefficient (R^2) between predicted and experimental shear capacities of 95.84 %. Considering the limited number of existing samples, further validation is required to assess the performance of the model. The equation $V_{pred} = 0.9V_{exp} + 9.61$ in Fig. 15 reflects the linear regression between V_{pred} and V_{exp}. The slope of 0.9 indicates that the model's predictions are slightly lower than the experimental values, and the intercept of 9.61 represents the constant offset between predicted and experimental shear strengths. This regression relationship provides a measure of the model's predictive accuracy. In addition, the predicted shear strength values for the five beams tested in this study are consistently lower than the experimental results, a trend that contrasts with the more random distribution observed in beams collected from other literature sources. This difference is attributed to the size effect, which is captured by the use of coefficient K in Eurocode 2 model for the shear strength of concrete (see Eq. (3)). However, coefficient K does not fully capture the nonlinear scaling effects of smaller cross-sections as highlighted by Bažant and Planas [69]. Fracture energy plays a more significant role in smaller beams, resulting in higher crack tip energy release rates and enhanced arching action [69]. This shift can cause prediction models to underestimate the shear capacity of small beams.

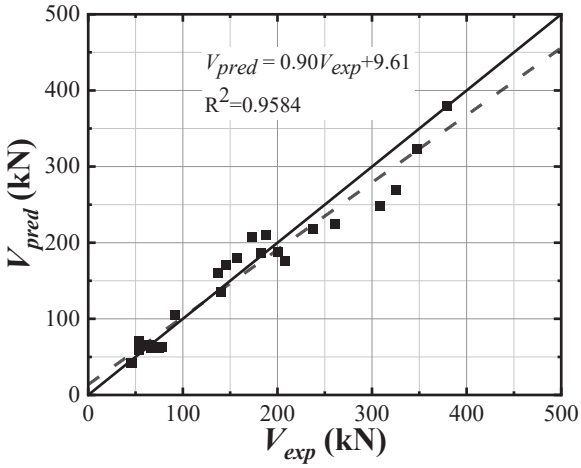

Fig. 15. Comparison between predicted and experimental shear strength.

In this study, the influence of a/d is is incorporated through correction factors R_c and R_f, derived from regression analysis of experimental data, as shown in Eqs. (18) and (19). These factors capture the distinct effects of a/d on beam shear capacity (arch or truss action) and SRG jacketing contribution. While the current model effectively incorporates these influences, the role of a/d in other formulations remains underexplored and warrants further investigation. Notably, the

Table 5
Experimental database of SRG strengthened RC beams and predicted shear strength.

	b_w (mm)	d (mm)	a/d	f_c' (MPA)	t_f (mm)	w_f/s_f	ρ_f (%)	E_f (GPA)	$\varepsilon_{fu,f}$	V_{exp} (kN)	V_{pred} (kN)	V_{pred}/V_{exp}
Present study												
A-GL-U2	102	177	2.0	22.2	0.084	1.00	0.329	190	0.015	74.9	62.2	0.83
A-GH-U1	102	177	2.0	22.1	0.169	1.00	0.331	190	0.015	66.5	62.2	0.94
A-GH-W1	102	177	2.0	22.7	0.169	1.00	0.331	190	0.015	73.4	62.7	0.85
B-GL-U2	102	177	3.5	20.5	0.084	1.00	0.329	190	0.015	44.8	41.5	0.93
B-GH-U1	102	177	3.5	22.2	0.169	1.00	0.331	190	0.015	45.8	42.6	0.93
Thermou et al. [12]												
BUL1	200	270	2.2	23.3	0.084	1.00	0.084	190	0.015	140.2	135.7	0.97
BUL2	200	270	2.2	23.3	0.084	1.00	0.168	190	0.015	136.6	160.2	1.17
BUML1	200	270	2.2	23.3	0.084	1.00	0.084	190	0.015	146.0	171.4	1.17
Wakjira & Ebead [32]												
BS1-L	180	334	3.1	34.0	0.084	1.00	0.187	190	0.015	157.1	180.3	1.15
BS1-H	180	334	3.1	34.0	0.169	1.00	0.376	190	0.015	187.7	209.6	1.12
BS2-L	180	334	2.6	34.0	0.084	1.00	0.376	190	0.015	237.5	218.7	0.92
BS2-H	180	334	2.6	34.0	0.084	1.00	0.376	190	0.015	260.8	224.0	0.86
BS3-L	180	334	2.1	34.0	0.084	1.00	0.187	190	0.015	308.9	249.0	0.81
BS3-H	180	334	2.1	34.0	0.169	1.00	0.376	190	0.015	325.7	269.1	0.83
BS4-L	180	334	1.6	34.0	0.084	1.00	0.187	190	0.015	347.0	323.5	0.93
BS4-H	180	334	1.6	34.0	0.169	1.00	0.376	190	0.015	379.3	379.3	1.00
Wakjira & Ebead [31]												
B1-U-L	180	335	2.8	34.0	0.084	1.00	0.187	190	0.015	207.9	176.2	0.85
B1-U-H	180	335	2.8	34.0	0.169	1.00	0.376	190	0.015	200.8	187.5	0.93
B1-S-L	180	335	2.8	34.0	0.084	1.00	0.187	190	0.015	182.3	186.3	1.02
B1-S-H	180	335	2.8	34.0	0.169	1.00	0.376	190	0.015	172.8	207.9	1.20
Ombres & Verre, [34]												
BC-2L	200	263	3.4	14.4	0.084	1.00	0.168	197.0	0.020	91.8	105.0	1.14
BD-1L−3S	200	263	3.4	14.4	0.084	0.29	0.024	197.0	0.020	53.7	59.1	1.10
BD-1L−4S	200	263	3.4	14.4	0.084	0.43	0.036	197.0	0.020	63.7	65.2	1.02
BD-2L−3S	200	263	3.4	14.4	0.084	0.29	0.048	197.0	0.020	77.8	63.4	0.81
BD-2L−4S	200	263	3.4	14.4	0.084	0.43	0.072	197.0	0.020	53.1	71.6	1.35

Note: V_{exp} = the experimental shear strength; V_{pred} = the predicted shear strength.

model's validity for low-strength concrete (below 17 MPa) should be carefully evaluated, as empirical formulas may not fully represent its behaviour [70]. Moreover, the high R^2 value observed between the predicted and experimental results not only indicates the model's ability to accurately capture the key parameters influencing shear strength but also reflects the limitations inherent to the dataset and assumptions. Considering the limited dataset, further experiments are necessary to expand the database and validate the model.

5. Conclusions

The study experimentally investigated the shear strengthening effectiveness of RC beams with different a/d ratios through external bonding of SRG. Through a comparison with the performance of CFRCM and SRP-strengthened beams, the efficacy of the SRG system was analysed. Seventeen two-span RC beams were constructed, divided into two groups based on different a/d ratios (2.0 and 3.5). Two beams served as control samples, while the rest were reinforced with U-shaped wrapping, full wrapping SRG, CFRCM and SRP jackets. In addition to a/d ratio and strengthening configuration, parameters included UHTSS textile density, layers of carbon textile, and different matrices. A predictive model was proposed, considering the impact of shear span ratio on the shear strength of both the concrete beams and the strengthening systems, for the shear capacity prediction of SRG-strengthened RC beams without stirrups. The main conclusions drawn from this study are as follows:

- All systems effectively enhanced the strength capacity of shear deficient RC beams. For beams with $a/d = 2.0$ (Series A beams), the strength increased by 90–124 % and 119–176 % for SRG and SRP systems, respectively. The shear strength increases in CFRCM strengthened beams was 107–174 %. For beams $a/d = 3.5$ (Series B beams), the strength increased by 164–170 % and 221 % for U-shaped SRG and SRP systems, respectively, while the shear strength increase in U-shaped CFRCM was 204–215 %.
- As the shear span ratio increased, a decrease in the shear strength of the strengthening system was observed, while the proportion of shear contribution provided by the strengthening system increased. This is related to the dominant shift in the load-carrying mechanism of the beam from an arch effect to a truss effect when transitioning from deep beams (Series A) to slender beams (Series B).
- Regarding the SRG systems, the utilization of UHTSS with a density of 3.14 cords/cm posed certain challenges in terms of the mortar's ability to penetrate the small gaps between successive cords. As a result, it is advisable to opt for textiles with lower density for similar applications. On the contrary, the implementation of UHTSS with a density of 3.14 cords/cm proved to be highly effective in the SRP jacketing application (i.e. resin matrix). In comparison, CFRCM and SRP systems demonstrate an advantage in shear strength enhancement, while the SRG system holds an advantage in improving ductility.
- All U-shaped jacketed beams exhibited shear-detachment failure independently of the type of jacket (SRG, SRP, CFRCM). However, in the case of SRP jacketing, detachment occurred by tearing off large parts of the concrete cover and concrete core due to the high adhesion offered by the resin matrix. The fully wrapped beams were able to modify the failure mode from brittle to ductile and demonstrated a high energy absorption capacity.
- The proposed analytical model, accounting for the influence of a/d, effectively predicts the shear capacity of SRG-strengthened, stirrup-free RC beams in the database. The average and standard deviation (STD) of $V_{pred}/V_{\exp}$ are 0.99 and 0.15.

In general, the research findings suggest that jacketing systems such as SRG, SRP, and CFRCM are effective techniques to strengthen shear-deficient RC beams. However, further investigations are needed to understand the interaction between internally and externally reinforcement system and to prevent detachment as a mode of failure in case of U-shaped jackets. Additionally, while the proposed model effectively incorporates the influence of a/d ratios through correction factors, its applicability to low-strength concrete (below 17 MPa) should be approached with caution. Considering the limited dataset, further experiments are necessary to expand the database and validate the model.

CRediT authorship contribution statement

Thermou Georgia: Writing – review & editing, Supervision, Methodology, Conceptualization. **Liu Xiangsheng:** Writing – original draft, Methodology, Investigation, Formal analysis, Data curation, Conceptualization.

Declaration of Competing Interest

The authors declare that they have no known competing financial interests or personal relationships that could have appeared to influence the work reported in this paper.

Acknowledgments

Special thanks are attributed to Kerakoll S.p.A. for providing the materials.

References

[1] Arslan M, Korkmaz HH. What is to be learned from damage and failure of reinforced concrete structures during recent earthquakes in Turkey? Eng Fail Anal 2007;14(1):1–22.
[2] Pardalopoulos SJ, Thermou GE, Pantazopoulou SJ. Screening criteria to identify brittle RC structural failures in earthquakes. Bull Earthq Eng 2013;11(2):607–36.
[3] Thermou G, Pantazopoulou SJ. Assessment indices for the seismic vulnerability of existing RC buildings. Earthq Eng Struct Dyn 2011;40(3):293–313.
[4] Galal K, Mofidi A. Strengthening RC beams in flexure using new hybrid FRP sheet/ductile anchor system. J Compos Constr 2009;13(3):217–25.
[5] Siddika A, Al Mamun MA, Alyousef R, Amran YM. Strengthening of reinforced concrete beams by using fiber-reinforced polymer composites: a review. J Build Eng 2019;25:100798.
[6] Thermou GE, Hajirasouliha I. Compressive behaviour of concrete columns confined with steel-reinforced grout jackets. Compos Part B: Eng 2018;138:222–31.
[7] Lu Y, Li W, Zhou Y, Mansour W, Zheng K, Wang P, Ke L, Yu J. Comparative analysis of shear behavior and mechanism of concrete beams with strip-shaped CFRP or conventional steel stirrups. Case Stud Constr Mater 2024;20:e03140.
[8] Wu M, Xu J, Li W, Li W, Wang C, Wang P. Axial compression behaviour of concrete columns with CFRP-mesh fabric (CFRP-MF) stirrup and steel-FRP composite bar (SFCB): experimental investigation and mechanism research. Constr Build Mater 2024;436:136853.
[9] Wu M, Xu J, Wang C, Wang P, Li W. Response of columns with steel–FRP composite bars and carbon fibre reinforced polymer mesh fabric stirrups under eccentric loading. Eng Struct 2024;316:118508.
[10] Wu M, Yuan F, Wang P, Li W. Concentrically loaded concrete columns reinforced with steel-FRP composite bars (SFCB) and carbon fibre-reinforced polymer mesh fabric (CFRP-MF) stirrups. Structures. Elsevier; 2024, 106794.
[11] Wei J, Ke L, Wang P, Li W, Leung CK. Microstructure, mechanical properties and interaction mechanism of seawater sea-sand engineered cementitious composite (SS-ECC) with Glass Fiber Reinforced Polymer (GFRP) bar. Compos Struct 2024;343:118302.
[12] Thermou G, Papanikolaou V, Lioupis C, Hajirasouliha I. Steel-Reinforced Grout (SRG) strengthening of shear-critical RC beams. Constr Build Mater 2019;216:68–83.
[13] Gonzalez-Libreros JH, Sabau C, Sneed LH, Pellegrino C, Sas G. State of research on shear strengthening of RC beams with FRCM composites. Constr Build Mater 2017;149:444–58.
[14] Wakjira TG, Ebead U. Internal transverse reinforcement configuration effect of EB/NSE-FRCM shear strengthening of RC deep beams. Compos Part B: Eng 2019;166:758–72.
[15] U. Ebead, T. Wakjira, FRCM/stirrups interaction in RC beams strengthened in shear using NSE-FRCM, IOP Conference Series: Materials Science and Engineering, IOP Publishing, 2018, p. 112001.
[16] A. Younis, U. Ebead, Characterization and application of FRCM as a strengthening material for shear-critical RC beams, MATEC Web of Conferences, EDP Sciences, 2018, p. 09004.
[17] Younis A, Ebead U, Shrestha KC. Different FRCM systems for shear-strengthening of reinforced concrete beams. Constr Build Mater 2017;153:514–26.

[18] Tzoura E, Triantafillou T. Shear strengthening of reinforced concrete T-beams under cyclic loading with TRM or FRP jackets. Mater Struct 2016;49(1):17–28.
[19] Triantafillou TC, Papanicolaou CG. Shear strengthening of reinforced concrete members with textile reinforced mortar (TRM) jackets. Mater Struct 2006;39(1):93–103.
[20] Tetta ZC, Koutas LN, Bournas DA. Shear strengthening of full-scale RC T-beams using textile-reinforced mortar and textile-based anchors. Compos Part B: Eng 2016;95:225–39.
[21] Tetta ZC, Koutas LN, Bournas DA. Shear strengthening of concrete members with TRM jackets: effect of shear span-to-depth ratio, material and amount of external reinforcement. Compos Part B: Eng 2018;137:184–201.
[22] Tetta ZC, Koutas LN, Bournas DA. Textile-reinforced mortar (TRM) versus fiber-reinforced polymers (FRP) in shear strengthening of concrete beams. Compos Part B: Eng 2015;77:338–48.
[23] Z. Tetta, Shear strengthening of concrete members with Textile Reinforced Mortar (TRM), University of Nottingham, 2017.
[24] Loreto G, Babaeidarabad S, Leardini L, Nanni A. RC beams shear-strengthened with fabric-reinforced-cementitious-matrix (FRCM) composite. Int J Adv Struct Eng (IJASE) 2015;7(4):341–52.
[25] Awani O, El-Maaddawy T, El Refai A. Numerical simulation and experimental testing of concrete beams strengthened in shear with fabric-reinforced cementitious matrix. J Compos Constr 2016;20(6):04016056.
[26] Aljazaeri ZR, Myers JJ. Strengthening of reinforced-concrete beams in shear with a fabric-reinforced cementitious matrix. J Compos Constr 2017;21(5):04017041.
[27] Marcinczak D, Trapko T, Musiał M. Shear strengthening of reinforced concrete beams with PBO-FRCM composites with anchorage. Compos Part B: Eng 2019;158:149–61.
[28] Gonzalez-Libreros JH, Sneed L, D'Antino T, Pellegrino C. Behavior of RC beams strengthened in shear with FRP and FRCM composites. Eng Struct 2017;150:830–42.
[29] Marcinczak D, Trapko T. DIC (Digital Image Correlation) method in the research of RC beams strengthened with PBO-FRCM materials, E3S Web of Conferences, EDP. Sciences 2019:03008.
[30] D. Marcinczak, T. Trapko, The impact of the anchorage on the shear capacity of reinforced concrete beams, IOP Conference Series: Materials Science and Engineering, IOP Publishing, 2019, p. 012003.
[31] Wakjira TG, Ebead U. Experimental and analytical study on strengthening of reinforced concrete T-beams in shear using steel reinforced grout (SRG). Compos Part B: Eng 2019;177:107368.
[32] Wakjira TG, Ebead U. Shear span-to-depth ratio effect on steel reinforced grout strengthened reinforced concrete beams. Eng Struct 2020;216:110737.
[33] Liu X, Thermou GE. A review on the shear performance of reinforced concrete (RC) beams strengthened with externally bonded mortar-based composites. Structures. Elsevier; 2023, 105474.
[34] Ombres L, Verre S. Shear strengthening of reinforced concrete beams with SRG (Steel Reinforced Grout) composites: experimental investigation and modelling. J Build Eng 2021;42:103047.
[35] Liu X, Thermou GE. Shear performance of RC beams strengthened with high-performance fibre-reinforced concrete (HPFRC) under static and fatigue loading. Materials 2024;17(21):5227.
[36] Li L, Zhang J, Li R, Ni X. Design oriented shear strength prediction model of UHPFRC beams. Structures. Elsevier; 2023, 105287.
[37] Muhammad JH, Mohmmad SH. Effect of shear span-to-depth ratio on shear strength of high-strength concrete beams reinforced with BFRP bars. Iran J Sci Technol, Trans Civ Eng 2024:1–16.
[38] Arowojolu O, Ibrahim A, Almakrab A, Saras N, Nielsen R. Influence of shear span-to-effective depth ratio on behavior of high-strength reinforced concrete beams. Int J Concr Struct Mater 2021;15:1–12.
[39] Shahnewaz M, Rteil A, Alam MS. Shear strength of reinforced concrete deep beams–A review with improved model by genetic algorithm and reliability analysis, Structures. Elsevier 2020:494–508.
[40] Sanal I. Effect of shear span-to-depth ratio on mechanical performance and cracking behavior of high strength steel fiber-reinforced concrete beams without conventional reinforcement. Mech Adv Mater Struct 2020;27(21):1849–64.
[41] Li W, Leung CK. Shear span–depth ratio effect on behavior of RC beam shear strengthened with full-wrapping FRP strip. J Compos Constr 2016;20(3):04015067.
[42] Bousselham A, Chaallal O. Behavior of reinforced concrete T-beams strengthened in shear with carbon fiber-reinforced polymer-an experimental study. Acids Struct J 2006;103(3):339.
[43] Shear A-ACo, Torsion. Recent approaches to shear design of structural concrete. J Struct Eng 1998;124(12):1375–417.
[44] Shafieifar M, Farzad M, Azizinamini A. A comparison of existing analytical methods to predict the flexural capacity of Ultra High Performance Concrete (UHPC) beams. Constr Build Mater 2018;172:10–8.
[45] Jung S, Kim KS. Knowledge-based prediction of shear strength of concrete beams without shear reinforcement. Eng Struct 2008;30(6):1515–25.
[46] Mandor A, El Refai A. Strengthening the hogging and sagging regions in continuous beams with fiber-reinforced cementitious matrix (FRCM): experimental and analytical investigations. Constr Build Mater 2022;321:126341.
[47] Al-Jaberi Z, Myers JJ. Prediction of compressive strength and evaluation of different theoretical standards and proposed models of brick columns confined with FRP, FRCM, or SRG system. Case Stud Constr Mater 2023;18:e01875.
[48] Cakir F, Aydin MR, Acar V, Aksar B, Akkaya HC. An experimental study on RC beams shear-strengthened with Intraply Hybrid U-Jackets Composites monitored by digital image correlation (DIC). Compos Struct 2023;323:117503.
[49] Ceroni F, Salzano P. Design provisions for FRCM systems bonded to concrete and masonry elements. Compos Part B: Eng 2018;143:230–42.
[50] B. En, 12390-13. Testing hardened concrete–Part 13: determination of secant modulus of elasticity in compression, British Standards Institution: London, UK (2013).
[51] U. ISO, 15630-1. Steel for the reinforcement and pre-stressing of concrete—test methods—part 1: reinforcing bars, wire rod and wire, AENOR: Madrid, Spain (2011).
[52] E. Iso, 6892-1. Metallic materials-Tensile testing-Part 1: Method of test at room temperature, International Organization for Standardization (2009).
[53] T. EN, 196-1. Methods of testing cement–Part 1: Determination of strength. Eur Comm Stand 2005;26.
[54] EN, Products and Systems for the Protection and Repair of Concrete Structures–Test Methods–Measurement of Bond Strength by Pull-Off, CEN Bruxelles, Belgium, 1999.
[55] B. EN, 12190. Products and systems for the protection and repair of concrete structures. Test methods. Determination of compressive strength of repair mortar, British Standards Institution: London, UK (1999).
[56] B. EN, 2561. Carbon fibre reinforced plastics. Undirectional laminates. Tensile test parallel to the fibre direction, British Standards Institution: London, UK (1995).
[57] Jabbar AM, Hamood MJ, Mohammed DH. The effect of using basalt fibers compared to steel fibers on the shear behavior of ultra-high performance concrete T-beam. Case Stud Constr Mater 2021;15:e00702.
[58] Lu WY, Lin IJ, Hwang SJ, Lin YH. Shear strength of high-strength concrete dapped-end beams. J Chin Inst Eng 2003;26(5):671–80.
[59] Ebead U. Inexpensive strengthening technique for partially loaded reinforced concrete beams: experimental study. J Mater Civ Eng 2015;27(10):04015002.
[60] Tan K-H, Cheng G-H, Zhang N. Experiment to mitigate size effect on deep beams. Mag Concr Res 2008;60(10):709–23.
[61] Européen C. Eurocode 2: Design of concrete structures—part 1-1: General rules and rules for buildings. London: British Standard Institution; 2004.
[62] Chen J, Teng J. Shear capacity of fiber-reinforced polymer-strengthened reinforced concrete beams: fiber reinforced polymer rupture. J Struct Eng 2003;129(5):615–25.
[63] Chen J-F, Teng J. Shear capacity of FRP-strengthened RC beams: FRP debonding. Constr Build Mater 2003;17(1):27–41.
[64] Rossi E, Randl N, Harsányi P, Mészöly T. Experimental study of fibre-reinforced TRC shear strengthening applications on non-stirrup reinforced concrete T-beams. Eng Struct 2022;256:113923.
[65] Tetta ZC, Triantafillou TC, Bournas DA. On the design of shear-strengthened RC members through the use of textile reinforced mortar overlays. Compos Part B: Eng 2018;147:178–96.
[66] Spinella N. Modeling of shear behavior of reinforced concrete beams strengthened with FRP. Compos Struct 2019;215:351–64.
[67] Escrig C, Gil L, Bernat-Maso E, Puigvert F. Experimental and analytical study of reinforced concrete beams shear strengthened with different types of textile-reinforced mortar. Constr Build Mater 2015;83:248–60.
[68] Kang TH-K, Ary MI. Shear-strengthening of reinforced & prestressed concrete beams using FRP: Part II—Experimental investigation. Int J Concr Struct Mater 2012;6(1):49–57.
[69] Bazant ZP, Planas J. Fracture and size effect in concrete and other quasibrittle materials. Routledge; 2019.
[70] Code A. 318-19; Building Code Requirements for Structural Concrete and Commentary. Farmington Hills, MI, USA: American Concrete Institute; 2019.